Superoxide Radical Anion Adduct of 5,5-Dimethyl-1-pyrroline *N*-Oxide. 5. Thermodynamics and Kinetics of Unimolecular Decomposition

Frederick A. Villamena[†]

Department of Pharmacology and Center for Biomedical EPR Spectroscopy and Imaging, The Davis Heart and Lung Research Institute, College of Medicine, The Ohio State University, Columbus, Ohio 43210

Received: March 13, 2009; Revised Manuscript Received: April 17, 2009

The unimolecular decomposition of the superoxide radical anion adducts of 5,5-dimethyl-1-pyrroline *N*-oxide (DMPO), 5-carbamoyl-5-methyl-1-pyrroline *N*-oxide (AMPO), 5-ethoxycarbonyl-5-methyl-1-pyrroline *N*-oxide (EMPO), and 5-diethoxyphosphoryl-5-methyl-1-pyrroline *N*-oxide (DEPMPO) were computationally investigated by using PCM/BHandLYP/6-311G(d,p)//B3LYP/6-31G(d) and PCM/ROMP2/cc-PVDZ//B3LYP/6-31G(d) levels of theory. Results indicate that the O−O bond scission for nitrone−O_2H to form the hydroxyl radical and the biradical is endoergic, and that the ring-opening step to form the nitrosoaldehyde is highly exoergic. The energy barriers for the O−O bond scission and ring-opening processes indicate that the former is the rate-limiting step of the reaction. The overall energetics for DMPO−O_2H decomposition in the presence and absence of explicit water interactions was found to be the most preferred; however, no significant differences in the energetics of decomposition among the various isomers of AMPO−O_2H, EMPO−O_2H, and DEPMPO−O_2H were observed.

I. Introduction

The unique ability of nitrones to form persistent radical adducts that are detectable and fingerprintable by electron paramagnetic resonance (EPR) spectroscopy has made nitrones a popular reagent for the detection and identification of transient radicals.[1] Spin trapping has contributed significantly toward the understanding of some of the fundamental radical-mediated mechanisms in chemical and biological systems.[2] The superoxide radical anion ($O_2^{\bullet-}$) is one of the most important reactive oxygen species (ROS) in biological systems and is a precurssor to highly reactive species (ROS) such as $HO^\bullet$, $ONOO^-$, and $GSSG^{\bullet-}$. ROS in unregulated concentrations can cause oxidative damage to cells,[3] and therefore detection of $O_2^{\bullet-}$ production in cellular systems is important.

Cyclic nitrones (Figure 1) are more preferred as probes for radical identification than the linear PBN-type nitrones due to the ability of cyclic nitrone spin adducts to exhibit distinctive and discernible EPR spectra. 5,5-Dimethyl-1-pyrroline *N*-oxide (DMPO)[4] is the most widely used spin-trap for the detection of $O_2^{\bullet-}$, but the $O_2^{\bullet-}$ adduct it forms has a short half-life of only ~1 min.[5,6] However, the $O_2^{\bullet-}$ adduct of the amide and ester substituted spin-traps such as 5-carbamoyl-5-methyl-1-pyrroline *N*-oxide (AMPO)[7] and 5-ethoxycarbonyl-5-methyl-1-pyrroline *N*-oxide (EMPO),[8] respectively, gave half-lives of $t_{1/2} \approx 8-10$ min while the alkoxyphoshorylated nitrone, 5-diethoxyphosphoryl-5-methyl-1-pyrroline *N*-oxide (DEPMPO),[9] gave the longest half-life of $t_{1/2} \approx 14$ min (see Table 1).

Our previous computational studies indicate that there is a significant energy preference between the formation of cis and trans adducts.[10] We postulated[11] that due to the pK_a of 4.8 for $O_2^{\bullet-}$ and that since spin trapping is typically carried out at pH 7.0, it can be assumed that the initial mechanism for nitrone−O_2H formation is via formation of nitrone−$O_2^{\bullet-}$. Since the calculated pK_a for DMPO−$O_2^{\bullet-}$ was found to be ~15, subsequent proton abstraction from water can occur (see Scheme
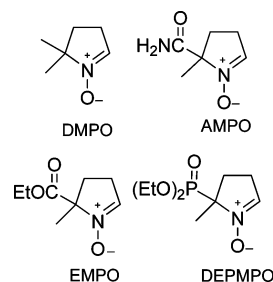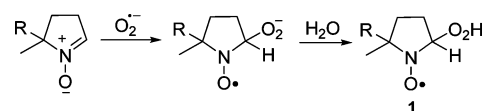

Figure 1. Examples of cyclic nitrone.

TABLE 1: Reported Experimental First-Order Half-Lives of the $O_2^{\bullet-}$ Adduct of Cyclic Nitrones

| adducts	$t_{1/2}$ (min)
DMPO−O_2H	1.0[6]
EMPO−O_2H	8.6[28]
DEPMPO−O_2H	14[29]
AMPO−O_2H	9.9[7]

SCHEME 1: Mechanism of Nitrone−O_2H Adduct in Neutral pH

1). Therefore, the major configuration for $HO_2^\bullet$ adduct is governed by the stereoselectivity of $O_2^{\bullet-}$ addition to the nitrone. From hereon, the $O_2^{\bullet-}$ adduct will be referred to as the $HO_2^\bullet$ adduct.

The mechanism of $HO_2^\bullet$ adduct decomposition can proceed via unimolecular and bimolecular pathways, but only first-order decay kinetics was observed for DMPO−O_2H during the whole course of its decomposition.[9,12] However, a mixture of first- and second-order decay kinetics were observed for the decomposition of the $HO_2^\bullet$ adducts of DEPMPO, AMPO, and EMPO, where bimolecular mechanism mostly occurs during the early

[†] E-mail: frederick.villamena@osumc.edu. Fax: (614)-688-0999.

Decomposition of the Superoxide Radical Anion Adducts

J. Phys. Chem. A, Vol. 113, No. 22, 2009 **6399**

SCHEME 2: Unimolecular Decomposition of the Hydroperoxyl Adduct of Nitrones
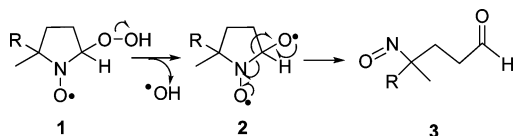
stage of decomposition due to the high adduct concentrations at these time points while first-order decay kinetics is more predominant at the later part of the decomposition.[7,9] Moreover, it should be noted that in all the previous kinetic studies,[7,9,12] the generation of $O_2^{\bullet-}$ was terminated either by addition of superoxide dismutase or turning off the light source for enzymatically or photochemically generated $O_2^{\bullet-}$, respectively, before any decay measurements were carried out as the reaction of $HO_2^{\bullet}/O_2^{\bullet-}$ to the $HO_2^{\bullet}$ adducts may facilitate adduct decomposition as observed for the more stable nitroxides such as TEMPO.[13] Since the half-lives shown in Table 1 were obtained from the later part of the decay plots showing first-order decay kinetics, these values are therefore reasonable approximations of the apparent half-lives for the unimolecular decomposition of the various $HO_2^{\bullet}$ adducts but the presence of other unknown unimolecular decomposition pathways should not be discounted.

We previously[14] showed that the unimolecular decomposition of DMPO–O_2H to nitrosoaldehyde (Scheme 2) is predicted to be thermodynamically favored in both gaseous and aqueous phases. We also experimentally showed that the decomposition of several $HO_2^{\bullet}$ adducts (**1**) yielded nitric oxide (NO) as a product[15] and may have pharmacological implications.[16] Although the unimolecular decomposition of the $O_2^{\bullet-}$ adduct of DMPO, DEPMPO, and EMPO has been experimentally investigated,[15] the trends in the activation barrier and thermodynamics of decomposition as shown in Scheme 2 have not been explored in detail. In this work, attempts to computationally rationalize the various half-lives of $HO_2^{\bullet}$ adducts through investigation of their kinetics and thermodynamics of decay as shown in Scheme 2 is presented.

II. Computational Methods

All calculations were performed with Gaussian 03[17] at the Ohio Supercomputer Center. Density functional theory (DFT)[18] at the B3LYP/6-31G(d) level of theory was employed in this study to determine the optimized geometry of the $HO_2^{\bullet}$ adducts, biradicals, and nitrosoaldehydes, and yielded no imaginary vibrational frequency. Spin adduct structures were chosen based on the most stable conformer/configurations in aqueous solution via polarizable continuum model (PCM) single-point energies on the gas-phase geometries[19] and were employed for the transition state (TS) search of the O–O bond scission process. These TS structures for the conversion of $HO_2^{\bullet}$ adduct to the biradical representing the O–O homolytic bond cleavage were confirmed to only have one imaginary vibrational frequency. A scaling factor of 0.9806[20] was used for the zero-point vibrational energy (ZPE) corrections for all the B3LYP/6-31G(d) geometries. Free energies were obtained from the calculated thermal and entropic corrections at 298 K, using the unscaled vibrational frequencies. The effects of solvation on the B3LYP/6-31G(d) gas-phase calculations were also investigated by using the PCM,[21] and the spin and charge densities were obtained from natural population analysis (NPA) approach[22] at the PCM/BHandLYP/6-311G(d,p) and PCM/ROMP2/cc-PVDZ levels of theory. Negligible spin contamination of $0.75 < \langle S^2 \rangle < 0.76$ was

TABLE 2: Bottom-of-the-Well Energy Barriers for the O–O Scission in DMPO–O_2H at Various Levels of Theory Based on B3LYP/6-31G(d) Optimized Structures unless Otherwise Indicated

level of theory	$\Delta E^{\ddagger}$ (0 K), kcal/mol
B3LYP/6-31+G(d,p)	25.3
BHandHLYP/6-311G(d,p)	56.5
BHandHLYP/cc-PVDZ	59.2
BHandHLYP/aug-ccPVDZ	52.0
ROMP2/6-311G(d,p)	23.8
ROMP2/cc-PVDZ	54.3
ROMP2/aug-ccPVDZ	48.2
QCISD/cc-PVDZ	55.6
BHandHLYP/6-311G(d,p)//BHandHLYP/6-31G(d)	41.6
PCM//BHandHLYP/6-311G(d,p)//BHandHLYP/6-31G(d)	56.6

obtained for the minima, while a moderate one ($0.78 < \langle S^2 \rangle < 1.11$) was obtained for the transition state structures and $\langle S^2 \rangle = 2.00$ for the triplet states.

III. Results and Discussion

A. Benchmark Studies. It has been shown by Krenske and Schiesser[23] that B3LYP-based approaches using small basis sets (cc-pVDZ or 6-31G(d)) gave lower estimates of the energy barriers for the addition of phosphonyl or acyl radicals to double bonds, and that the BHandHLYP functional provided reasonable estimates to the higher level barriers. They also found that BHandHLYP, using the basis sets cc-pVDZ or 6-311G(d,p), gave similar estimates as the QCISD or CCSD(T) single-point calculations. However, attempts to find TS structures by using BHandHLYP/6-311G(d,p) for the activation barrier of the O–O scission in DMPO–O_2H failed for some of the adducts perhaps due to the size of the molecules, and therefore a comparative study of the energetics of all the various adducts is not possible. Transition state structure search at the B3LYP/6-31G(d) level was successful for all compounds and attempts to improve the energetics by using various single-point calculations were carried out. For benchmarking purposes, single-point energies were obtained by using various levels of theories as shown in Table 2. The B3LYP/6-31+G(d,p) and ROMP2/6-311G(d,p) levels gave the lowest estimate of the energy barriers while the BHandHLYP/6-311G(d,p)//B3LYP/6-31G(d) and ROMP2/cc-PVDZ//B3LYP/6-31G(d) gave bottom-of-the-well energy barrier estimates that are close to those of the more accurate QCISD/cc-PVDZ//B3LYP/6-31G(d) level. Moreover, a reasonable estimate was also obtained with PCM/BHandHLYP/6-311G(d,p)//BHandHLYP/6-31G(d) and a slighty lower estimate was obtained with the BHandHLYP/6-311G(d,p)/BHandHLYP/6-31G(d) level, which was preferred by Krenske and Schiesser.[23] Therefore, the use of both BHandHLYP/6-311G(d,p)//B3LYP/

SCHEME 3: O–O Bond Scission from $HO_2^{\bullet}$ Adduct Leading to the Formation of Singlet and Triplet Biradical Products
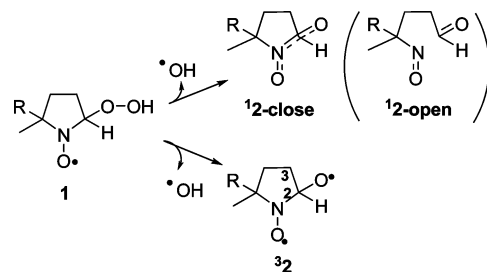
TABLE 3: Reaction Free Energies ($\Delta G_{\text{rxn,aq}}$) and Enthalpies (ΔH_{rxn} in parentheses) (in kcal/mol) for the Formation of Singlet (^{1}2-open and ^{1}2-close) and Triplet Biradical Species (^{3}2) via Loss of Hydroxyl Radical from the HO$_2$$^{\bullet}$ Adducts (1) of Various Cyclic Nitrones in Aqueous Phases at the PCM/BHandLYP/6-311G(d,p)//B3LYP/6-31G(d) and PCM/ROMP2/cc-PVDZ//B3LYP/6-31G(d) Levels of Theory
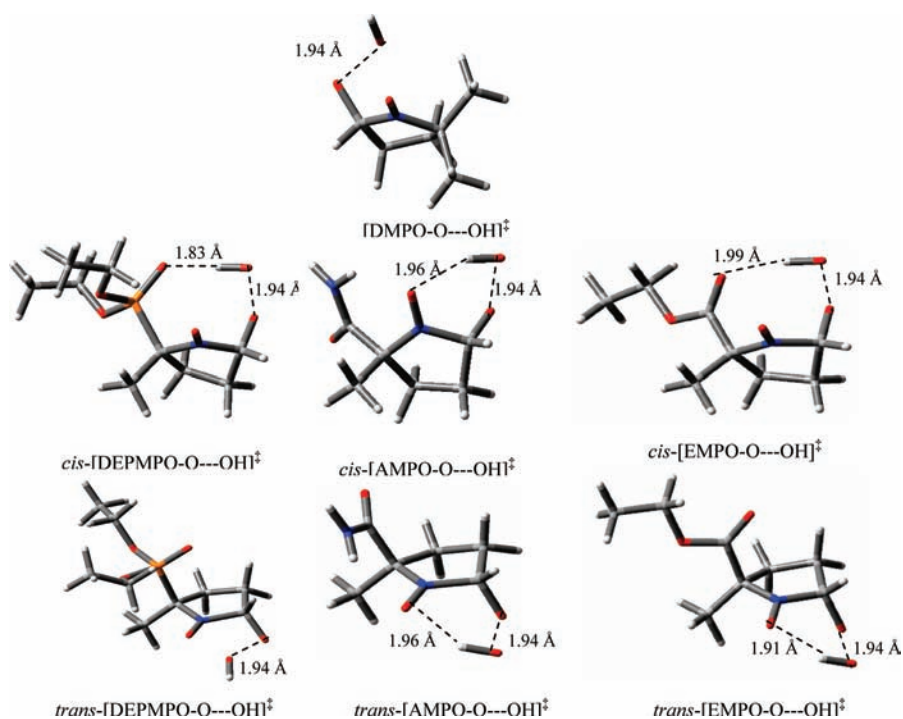
| | $\Delta G_{\text{rxn,aq}}$ ($\Delta H_{\text{rxn,aq}}$), kcal/mol | | | | | |
| | PCM/BHandLYP/6-311G(d,p)//B3LYP/6-31G(d) | | | ROMP2/cc-PVDZ//B3LYP/6-31G(d) | | |
compd	^{1}2-close	^{3}2	^{1}2-open	^{1}2-close	^{3}2	^{1}2-open
DMPO−O$_2$H	15.4 (25.2)	18.5 (29.4)	−3.5 (8.8)	2.5 (12.2)	−13.0 (−2.1)	−30.6 (−18.3)
AMPO−O$_2$H-*cis*	23.8 (33.4)	15.6 (26.7)	−2.6 (10.0)	12.5 (22.1)	−17.3 (−6.1)	−30.6 (−18.1)
AMPO−O$_2$H-*trans*	28.6 (38.1)	19.7 (30.5)	−1.8 (10.9)	18.6 (28.1)	−11.8 (−1.0)	−29.4 (−16.6)
DEPMPO−O$_2$H-*cis*	25.3 (36.7)	18.9 (31.4)	−0.8 (13.0)	13.3 (24.7)	−12.7 (−0.2)	−27.6 (−13.8)
DEPMPO−O$_2$H-*trans*	25.9 (35.8)	19.4 (30.1)	−1.7 (10.3)	13.6 (23.5)	−12.1 (−1.4)	−28.5 (−16.5)
EMPO−O$_2$H-*cis*	24.2 (34.5)	18.1 (30.2)	−4.7 (7.9)	11.9 (22.2)	−14.6 (−2.5)	−31.9 (−19.2)
EMPO−O$_2$H-*trans*	24.8 (34.3)	19.1 (29.9)	−3.7 (8.0)	12.8 (22.3)	−12.5 (−1.7)	−30.4 (−18.7)

6-31G(d) and ROMP2/cc-PVDZ//B3LYP/6-31G(d) levels of theory should justify calculation of approximated energetics of decomposition in this study.

B. Thermodynamics of O−O Bond Scission. Table 1 shows the previously reported experimental unimolecular half-lives for various HO$_2$$^{\bullet}$ adducts in which DMPO−O$_2$H and DEPMPO−O$_2$H showed the shortest and longest half-lives, respectively. Experimental evidence shows that the decomposition of DMPO−O$_2$H results in the formation of hydroxyl (HO$^{\bullet}$) adduct, and this was also observed from the HO$_2$$^{\bullet}$ adducts of DEPMPO and EMPO.[7] The formation of HO adduct from HO$_2$$^{\bullet}$ adduct was rationalized to be due to the homolytic scission of the O−O bond of the hydroperoxyl moiety. We previously[15] showed that the unimolecular decomposition of HO$_2$$^{\bullet}$ adduct **1** involves the release of HO$^{\bullet}$ to give an unstable biradical intermediate **2** that subsequently undergoes ring-opening to form a nitrosoaldehyde **3** as shown in Scheme 2. Compound **3** can then undergo C−N bond scission to release NO.

Attempts to optimize cyclic ^{1}**2** structures without bond restrictions failed and only resulted in ring-opening for some of the adducts. For the ^{1}**2** that optimized with a ring structure, the C−N bond distances where found to be between 1.52 and
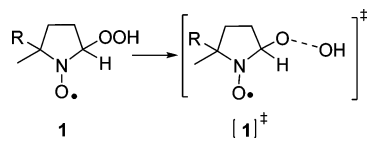
1.55 Å. Successful optimization of the remaining ^{1}**2** structures at fixed C−N bond distances of 1.56 Å was achieved and will be referred to as ^{1}**2-close**. On the other hand, optimization of ^{3}**2** without bond restrictions gave a ring structure with a C−N bond distance range of 1.48−1.49 Å for all the adducts except for ^{3}DMPO−O$^{\bullet}$, which gave a C−N bond distance of 1.53 Å. That the C−N bond length value for ^{3}DMPO−O$^{\bullet}$ is longer than that for the rest of the adducts implies that the ^{3}DMPO−O$^{\bullet}$ may be more susceptible to the C−N bond breaking process. Table 3 shows the free energies and enthalpies for the homolytic O−O bond cleavage of the hydroperoxyl moiety in **1** to form the singlet ^{1}**2-close** and triplet ^{3}**2** biradical (see Scheme 3). The magnitude of calculated singlet−triplet gap varies from one adduct to another, but in general, ^{3}**2** is more thermodynamically preferred than ^{1}**2-close** except for DMPO−O$^{\bullet}$ in which the ^{1}DMPO−O$^{\bullet}$ is more preferred by ∼3.0 kcal/mol compared to ^{3}DMPO−O$^{\bullet}$ at the PCM/BHandLYP/6-311G(d,p)//B3LYP/6-31G(d) level of theory. In general, the energetics of O−O bond scission are more exergic at PCM/ROMP2/cc-PVDZ//B3LYP/6-31G(d) compared to PCM/BHandLYP/6-311G(d,p)//B3LYP/6-31G(d). While the ^{1}**2-close** is more preferred than the ^{3}**2** state and that the ^{1}**2-close**-^{3}**2** gap is smallest for DMPO−O$^{\bullet}$ suggest

Figure 2. Transition state structures for the O−O bond scission for various HO$_2$$^{\bullet}$ adducts [**1**]‡ at the B3LYP/6-31G(d) level of theory.

Decomposition of the Superoxide Radical Anion Adducts

J. Phys. Chem. A, Vol. 113, No. 22, 2009 **6401**

TABLE 4: Activation Free Energies ($\Delta G^{\ddagger}_{298K,aq}$) and Enthalpies ($\Delta H^{\ddagger}_{298K,aq}$), Transition State C–N and O–O Bond Distances, and Imaginary Frequencies for the Homolytic O–O Bond Cleavage of Various HO$_2^{\bullet}$ Adducts at the PCM/BHandLYP/6-311G(d,p)//B3LYP/6-31G(d) and ROMP2/cc-PVDZ//B3LYP/6-31G(d) (in parentheses) Levels of Theory

structure	$\Delta H_{298K,aq}$, kcal/mol	$\Delta G_{298K,aq}$, kcal/mol	C---N, Å	O---O, Å	imaginary freq, $\langle S \rangle^2$
		DMPO			
1	0	0	1.46	1.46	0, 0.75
[**1**]‡	49.2 (54.5)	49.6 (54.9)	1.48	1.94	519i, 0.78
		cis-AMPO			
1	0.0	0.0	1.47	1.46	0, 0.75
[**1**]‡	22.9 (50.7)	23.2 (51.0)	1.48	1.94	353i, 0.78
		trans-AMPO			
1	0.0	0.0	1.47	1.46	0, 0.75
[**1**]‡	39.3 (50.9)	39.7 (51.3)	1.48	1.94	344i, 0.78
		cis-DEPMPO			
1	0.0	0.0	1.46	1.45	0, 0.75
[**1**]‡	24.4 (52.4)	24.5 (52.6)	1.48	1.94	526i, 1.11
		trans-DEPMPO			
1	0.0	0.0	1.47	1.46	0, 0.75
[**1**]‡	40.4 (47.2)	41.6 (48.4)	1.54	1.94	676i, 0.83
		cis-EMPO			
1	0.0	0.0	1.46	1.45	0, 0.75
[**1**]‡	40.3 (51.9)	40.3 (51.9)	1.47	1.94	554i, 1.08
		trans-EMPO			
1	0.0	0.0	1.47	1.46	0, 0.75
[**1**]‡	20.1 (50.5)	23.1 (50.6)	1.48	1.94	343i, 0.78

the preference for DMPO–O$_2$H to undergo O–O homolytic cleavage compared to the other HO$_2^{\bullet}$ adducts. However, although DMPO–O$_2$H has the least endoergic formation of ^{1}**2-close**, the calculated energies do not explain the long half-life observed for DEPMPO–O$_2$H since the energetics of formation of ^{1}DEPMPO–O$^{\bullet}$ (close) is similar to that of other ^{1}**2-close** structures. Spin densities at the PCM/BHandLYP/6-311G(d,p) level were also calculated by using natural population analysis (NPA)[24] and did not vary significantly on ^{3}**2** structures. The average spin density values of 0.45 ± 0.02, 0.54 ± 0.02, -0.08 ± 0.00, 0.09 ± 0.00, and 0.94 ± 0.00 e on the nitronyl-N,

nitronyl-O, C-2, C-3, and β-O, respectively, were obtained. The ^{3}**2** structures gave considerably higher electron density on C-3 with practically no spin density (-0.08 e) on C-2.
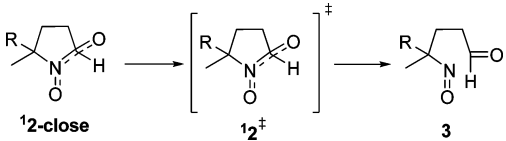
Optimization of ^{1}**2** without bond restrictions led to an open ring system with C–N bond distances of 3.0 Å for all of the adducts except for ^{1}EMPO–O$_2$H-*cis* with 4.1 Å. These open ring singlet state structures are referred to as ^{1}**2-open** in Table 3. Conversion of **1** to ^{1}**2-open** is mostly exoergic with $\Delta G_{rxn,aq}$ ranging from -0.8 to -4.7 kcal/mol at the PCM/BHandLYP/ 6-311G(d,p)//B3LYP/6-31G(d) level, but unlike in the conversion of **1** to ^{1}**2-close**, no correlation of the energetics with the observed half-lives can be observed as ^{1}DMPO–O$_2$H gave $\Delta G_{rxn,aq} = -3.5$ kcal/mol. No trends in the energetics was observed at the PCM/ROMP2/cc-PVDZ//B3LYP/6-31G(d) level.

C. Kinetics of O–O Bond Scission. The transition state (TS) structures for the O–O bond cleavage (i.e., **1** → **2**) were explored to investigate the effect of the energy barrier for this process on the observed half-lives. Figure 2 shows the various HO$_2^{\bullet}$ adduct TS structures **1**‡, and Table 4 shows the calculated O–O bond distances for **1** and ^{1}**1**‡ as well as their relative free energies and enthalpies. The energy barrier from **1** to **1**‡ is highest for DMPO–O$_2$H with $\Delta G_{rxn,aq} = 49.6$ kcal/mol at the PCM/BHandLYP/6-311G(d,p)//B3LYP/6-31G(d) level. The energy barriers of decomposition for various diastereoisomers (i.e., cis versus trans) vary significantly. For example, energy barriers are lower for AMPO–O$_2$H-*cis*, DEPMPO–O$_2$H-*cis*, and EMPO–O$_2$H-*trans* compared to their respective diasteriomers and may have consequences for the differences in their half-lives. Indeed, EPR line width asymmetry during HO$_2^{\bullet}$ adduct decomposition has been experimentally observed suggesting a difference in the half-lives of various diastereomers in solution.[25] The high activation barrier for DMPO–O$_2$H, however, does not explain its short half-life compared to other adducts and may indicate that the observed half-lives for various HO$_2^{\bullet}$ adducts may be thermodynamically controlled than kinetically. However, examination of the spin density distribitions in the TS structures at the PCM/BHandLYP/6-311G(d,p) (see Table 5) level shows significant electron delocalization on the –OH oxygen (65%) compared to other atoms in [DMPO–O$_2$H]‡ and [DEPMPO–O$_2$H-*trans*]‡, while almost equal electron distribution between the aminoxyl-O and -N was observed for the other **1**‡ structures characteristic of the spin density distribution expected in aminoxyl-NO's. According to the Hammond postulate, these differences in the spin density distribution profile for various HO$_2^{\bullet}$ adducts suggest a "product-like" TS for [DMPO–O$_2$H]‡

TABLE 5: Calculated Spin and Charge Densities (in parentheses) of the Various TS Structures (1‡) at the PCM/BHandLYP/ 6-311G(d,p)//B3LYP/6-31G(d) and PCM/ROMP2/cc-PVDZ//B3LYP/6-31G(d) Level of Theory

	spin and charge densities (in parentheses), e							
	PCM/BHandLYP/6-311G(d,p)//B3LYP/6-31G(d)				ROMP2/cc-PVDZ//B3LYP/6-31G(d)			
	O$_{aminoxyl}$	**N**$_{aminoxyl}$	**O**$_{(C-O)}$	**O**$_{(O-H)}$	**O**$_{aminoxyl}$	**N**$_{aminoxyl}$	**O**$_{(C-O)}$	**O**$_{(O-H)}$
DMPO	-0.18	0.17	0.39	0.65	0.00	0.00	0.13	0.86
	(-0.19)	(0.28)	(-0.69)	(-0.77)	(-0.20)	(0.29)	(-0.93)	(-0.58)
cis-AMPO	0.49	0.50	0.79	-0.82	0.53	0.43	0.01	0.00
	(-0.48)	(-0.00)	(-0.31)	(-0.46)	(-0.45)	(-0.09)	(-0.41)	(-0.47)
trans-AMPO	0.49	0.49	0.04	-0.03	0.54	0.42	0.01	0.00
	(-0.47)	(-0.00)	(-0.35)	(-0.48)	(-0.44)	(-0.09)	(-0.41)	(-0.47)
cis-DEPMPO	0.56	0.44	0.79	-0.82	0.65	0.31	0.01	0.00
	(-0.42)	(-0.04)	(-0.33)	(-0.48)	(-0.34)	(-0.17)	(-0.46)	(-0.46)
trans-DEPMPO	-0.12	0.07	0.44	0.64	0.00	0.00	0.13	0.86
	(-0.23)	(0.27)	(-0.66)	(-0.75)	(-0.22)	(0.30)	(-0.94)	(-0.57)
cis-EMPO	0.58	0.41	0.02	0.01	0.68	0.28	0.01	0.00
	(-0.40)	(-0.04)	(-0.37)	(-0.49)	(-0.31)	(-0.18)	(-0.42)	(-0.48)
trans-EMPO	0.52	0.48	-0.75	0.82	0.58	0.38	0.01	0.00
	(-0.45)	(-0.01)	(-0.32)	(-0.47)	(-0.40)	(-0.11)	(-0.41)	(-0.47)

TABLE 6: Enthalpies (ΔH_rxn,aq), Free Energies (ΔG_rxn,aq), C−N Bond Distances, and Imaginary Frequencies for the Formation of Nitrosoaldehyde (3) from Singlet Biradical (¹2-close) at the PCM/BHandLYP/6-311G(d,p)//B3LYP/6-31G(d) Level of Theory

structure	ΔH_298K,aq, kcal/mol	ΔG_298K,aq, kcal/mol	C---N, Å	imaginary freq
		DMPO		
¹2[a]	0.0	0.0	1.56	0
[¹2]‡	−3.3	−3.2	1.86	149i
3[b]	−23.5	−26.1	2.84	0
		cis-AMPO		
¹2	0.0	0.0	1.56	0
[¹2]‡	−2.0	−1.5	1.69	213i
3	−20.3	−22.7	2.99	0
		trans-AMPO		
¹2	0.0	0.0	1.52	0
[¹2]‡	−8.8	−10.1	1.86	163i
3	−27.2	−30.7	3.09	0
		cis-DEPMPO		
¹2	0.0	0.0	1.56	0
[¹2]‡	−8.4	−8.9	1.86	180i
3	−26.9	−28.5	2.85	0
		trans-DEPMPO		
¹2	0.0	0.0	1.56	0
[¹2]‡	−7.1	−6.1	1.86	156i
3	−25.4	−27.6	2.99	0
		cis-EMPO		
¹2	0.0	0.0	1.56	0
[¹2]‡	−5.8	−5.6	1.86	188i
3	−25.3	−27.8	3.19	0
		trans-EMPO		
¹2	0.0	0.0	1.56	0
[¹2]‡	−9.8	−9.3	1.86	181i
3	−26.2	−28.3	3.02	0

[a] All energies for ¹2 are from structures optimized at fixed C−N bond. [b] All energies for 3 are from structures resulting from 10% displacement of the transition state structures. $\langle S \rangle^2$ are all zero.

and [DEPMPO−O₂H-*trans*]‡ and "reagent-like" TS for the other 1‡'s, consistent with the high energy barriers predicted for [DMPO−O₂H]‡ and [DEPMPO−O₂H-*trans*]‡. A similar trend in the spin density distribution in 1‡ was observed at the ROMP2/cc-PVDZ level of theory.

D. Thermodynamics and Kinetics of C−N Bond Scission. The ring-opening step was further explored to investigate if there is any correlation between the energy barriers from this process to the observed half-lives. In this study, due to the difficulty in finding the ¹2‡ based on the most preferred 1 conformations, a TS search for ¹2‡ was independently performed and the 3 structures were obtained from the 10% displacement of the ¹2‡ structures and therefore may not reflect the overall energetics of ring opening (i.e., ¹2-close → 3) shown in Table 3. Table 6 also shows the C−N bond distances for ¹2-close, ¹2‡, and 3. The potential energy surfaces for the formation of 3 from ¹2-close for all of the adducts were barrierless except for EMPO-*cis* with a barrier of about ∼7 kcal/mol. The formation of 3 from ¹2‡ was all exoergic with ΔG_rxn,aq ranging from −21.9 to −37.2 kcal/mol. The trend in exoergicity for the conversion of ¹2-close (or ¹2‡) to 3 for all the adducts does not follow the trend in the experimental rate constants but nevertheless demonstrates the favorability of the ring-opening step after O−O bond scission from 1. That the energy barriers calculated for 1‡ are endoergic compared to those for ¹2‡ suggests that the O−O bond scission is therefore the rate-limiting step for the unimolecular decomposition of 1.

E. Overall Energetics of Decomposition in the Presence and Absence of Explicit Water Interaction. The overall enthalpies and free energies of formation of 3 from 1 (Scheme 2) in the presence of bulk dielectric effect of water were calculated and are shown in Table 7. In this study, a conformation search for 3 structures via a Monte Carlo method coupled with MMFF and further optimization at the B3LYP/6-31G(d) level of theory was carried out. A qualitative trend can be observed at the PCM/BHandLYP/6-311G(d,p)//B3LYP/6-31G(d) level of theory in which the formation of 3 from DMPO−O₂H is the most exoergic with ΔG_rxn,aq of −13.1 kcal/mol compared to other adducts with ΔG_rxn,aq ranging from −2.1 to −6.3 kcal/mol. The same trend in energetics was observed at the PCM/ROMP2/cc-PVDZ//B3LYP/6-31G(d) level of theory although they were more exoergic in general. However, the results still do not explain the long half-life observed for DEPMPO−O₂H because the ΔG_rxn,aq of −4.7 and −2.3 kcal/mol for the decomposition of its cis and trans isomers, respectively, are almost comparable to those predicted for EMPO−O₂H and AMPO−O₂H.

The effect of explicit water interaction on the energetics of formation of 3 from 1 was then investigated. Complexes of two explicit water molecules with 1 or 3 were optimized via a Monte Carlo method coupled with MMFF, and were further optimized at the B3LYP/6-31G(d) level of theory. Energies were further refined by taking into account the bulk dielectric effect of water using single-point energy calculations at the PCM/B3LYP/6-

TABLE 7: Reaction Free Energies (ΔG_rxn,aq) and Enthalpies (ΔH_rxn,aq) (in kcal/mol) for the Unimolecular Decomposition of Various Cyclic Nitrones (1 → 3) in Aqueous Phases at the PCM/BHandLYP/6-311G(d,p)//B3LYP/6-31G(d) and PCM/ROMP2/cc-PVDZ//B3LYP/6-31G(d) Levels of Theory[b]

	PCM/BHandLYP/6-311G(d,p)//B3LYP/6-31G(d)		ROMP2/cc-PVDZ//B3LYP/6-31G(d)	
compd[a]	ΔH_rxn,aq	ΔG_rxn,aq	ΔH_rxn,aq	ΔG_rxn,aq
DMPO−O₂H	−0.2 (4.4)	−13.1 (−8.4)	−27.8 (−24.3)	−40.7 (−37.1)
AMPO−O₂H-*cis*	7.1 (12.0)	−6.3 (0.6)	−21.3 (−15.7)	−34.7 (−27.2)
AMPO−O₂H-*trans*	10.9 (10.0)	−2.1 (−1.9)	−16.4 (−17.1)	−29.4 (−29.0)
DEPMPO−O₂H-*cis*	10.2 (7.4)	−4.7 (−4.7)	−17.5 (−21.5)	−32.4 (−33.5)
DEPMPO−O₂H-*trans*	10.1 (5.8)	−2.3 (−6.8)	−17.5 (−23.5)	−29.9 (−36.2)
EMPO−O₂H-*cis*	7.9 (8.8)	−4.9 (−4.8)	−19.5 (−18.8)	−32.3 (−32.4)
EMPO−O₂H-*trans*	8.0 (11.5)	−3.7 (−0.3)	−18.7 (−15.9)	−30.4 (−27.7)

[a] Based on the most favorable 1 and 3 conformers. [b] Values in parentheses are energies in the presence of two explicit water molecules in 1 and 3 at the same level of theory.

Decomposition of the Superoxide Radical Anion Adducts

J. Phys. Chem. A, Vol. 113, No. 22, 2009 **6403**

31+G(d,p) level. The energetics of formation of **3** from **1** were calculated and are shown in Table 7 (in parentheses). In general, the free energies of decomposition of $HO_2^•$ adducts in the presence and absence of explicit water molecules are similar but the trends in energies still show that the decomposition of $DMPO-O_2H·(H_2O)_2$ is the most exoergic. No significant improvement in the correlation between the trends in free energies and experimentally observed half-lives occurs when only the most exoergic decomposition pathways are considered for each adducts, that is, formation of **3** from *cis*-AMPO$-O_2H$, *cis*-DEPMPO$-O_2H$, and *cis*-EMPO$-O_2H$.

Although this study successfully rationalized the short half-life of DMPO$-O_2H$ compared to other adducts, it does not explain the long half-life observed for DEPMPO$-O_2H$ as its energetics shown so far are comparable to those of AMPO$-O_2H$ and EMPO$-O_2H$. Different intramolecular H-bonding motifs such as hydroperoxyl-H interaction with nitronyl-O, carbonyl-O, phosphoryl-O, and carbamoyl-N have been previously predicted[26] for various $HO_2^•$ adducts and this intramolecular interaction could also play a role in their stabilization. The $-O_2H$---O═P bond distance observed in DEPMPO$-O_2H$ is the shortest (1.82 Å) compared to the 1.99$-$2.09 Å distances observed for $-O_2H$---O-N, $-O_2H$---N, and $-O_2H$---O═C bonds. The differences in bond distances are supported by infrared (IR) studies[27] which show that the P═O group is a two orders of magnitude stronger H-bond acceptor than the C═O group. However, the thermodynamic and kinetic data for the O$-$O bond scission process do not reflect the relative strenghts of these intramolecular H-bonding interactions. In fact, the free energies of O$-$O bond scission for *cis*- and *trans*-DEPMPO$-O_2H$ are similar as shown in Table 3. However, the contribution of other conformational isomers on the overall energetics was not considered in this study and therefore future efforts in predicting the half-lives of the $HO_2^•$ adducts should take into account the Boltzmann averaging of the various conformational isomers for each of the cis and trans adducts.

IV. Conclusions

A computational approach was used to analyze the unimolecular decomposition of various cyclic nitrones. The formation of the singlet or triplet biradical species from the loss of HO$^•$ from the $HO_2^•$ adducts was predicted to be endoergic. The decomposition of the singlet biradical to the corresponding nitrosoaldehyde is a barrierless process and is highly exoergic. The decomposition of DMPO$-O_2H$ is the most exoergic from thermodynamic considerations compared to other $HO_2^•$ adducts. The total energy yielded modest results that explain the long half-lives of DEPMPO$-O_2H$, EMPO$-O_2H$, and AMPO$-O_2H$ compared to DMPO$-O_2H$. However, only a small improvement in trends of the overall energetics of decomposition was observed when explicit water molecule interaction with the $HO_2^•$ adducts and the final nitrosoaldehyde products were considered.

Note Added after ASAP Publication. This paper was published ASAP on May 8, 2009. An entry in Table 3 was changed. The revised paper was reposted on May 13, 2009.

Supporting Information Available: Bottom-of-the-well energies, free energies, and enthalpies for all the compounds. This material is available free of charge via the Internet at http://pubs.acs.org.

References and Notes

(1) (a) Janzen, E. G. *Acc. Chem. Res.* **1971**, *4*, 31–40. (b) Janzen, E. G.; Haire, D. L. *Adv. Free Radical Chem.* **1990**, *1*, 253–295. (c) Villamena, F. A.; Zweier, J. L. *Antioxid. Redox Signaling* **2004**, *6*, 619–629.

(2) (a) Zweier, J. L.; Flaherty, J. T.; Weisfeldt, M. L. *Proc. Natl. Acad. U.S.A.* **1987**, *84*, 1404. (b) Zweier, J. L.; Kuppusamy, P.; Lutty, G. A. *Proc. Natl. Acad. U.S.A.* **1988**, *85*, 4046.

(3) Halliwell, B.; Gutteridge, J. M. C. *Free Radicals in Biology and Medicine*; Oxford University Press: New York, 1999.

(4) (a) Iwamura, M.; Inamoto, N. *Bull. Chem. Soc. Jpn.* **1967**, *40*, 703. (b) Janzen, E. G.; Blackburn, B. J. *J. Am. Chem. Soc.* **1968**, *90*, 5909.

(5) (a) Buettner, G. R.; Oberley, L. W. *Biochem. Biophys. Res. Commun.* **1978**, *83*, 69–74. (b) Finkelstein, E.; Rosen, G. M.; Rauckman, E. J. *Mol. Pharmacol.* **1982**, *21*, 262–265. (c) Finkelstein, E.; Rosen, G. M.; Rauckman, E. J. *J. Am. Chem. Soc.* **1980**, *102*, 4994–4999.

(6) Finkelstein, E.; Rosen, G. M.; Rauckman, E. J. *Mol. Pharmacol.* **1979**, *16*, 676–685.

(7) Villamena, F. A.; Rockenbauer, A.; Gallucci, J.; Velayutham, M.; Hadad, C. M.; Zweier, J. L. *J. Org. Chem.* **2004**, *69*, 7994–8004.

(8) Olive, G.; Mercier, A.; Le Moigne, F.; Rockenbauer, A.; Tordo, P. *Free Radical Biol. Med.* **2000**, *28*, 403–408.

(9) Frejaville, C.; Karoui, H.; Tuccio, B.; Le Moigne, F.; Culcasi, M.; Pietri, S.; Lauricella, R.; Tordo, P. *J. Med. Chem.* **1995**, *38*, 258–265.

(10) Villamena, F. A.; Xia, S.; Merle, J. K.; Lauricella, R.; Tuccio, B.; Hadad, C. M.; Zweier, J. L. *J. Am. Chem. Soc.* **2007**, *129*, 8177–8191.

(11) Villamena, F. A.; Merle, J. K.; Hadad, C. M.; Zweier, J. L. *J. Phys. Chem. A* **2005**, *109*, 6083–6088.

(12) Villamena, F. A.; Zweier, J. L. *J. Chem. Soc., Perkin Trans. 2* **2002**, 1340–1344.

(13) Goldstein, S.; Merenyi, G.; Russo, A.; Samuni, A. *J. Am. Chem. Soc.* **2003**, *125*, 789–795.

(14) Villamena, F. A.; Merle, J. K.; Hadad, C. M.; Zweier, J. L. *J. Phys. Chem. A* **2005**, *109*, 6089–6098.

(15) Locigno, E. J.; Zweier, J. L.; Villamena, F. A. *Org. Biomol. Chem.* **2005**, *3*, 3220–3227.

(16) Zuo, L.; Chen, Y. R.; Reyes, L. A.; Lee, H. L.; Chen, C. L.; Villamena, F. A.; Zweier, J. L. *J. Pharmacol. Exp. Ther.* **2009**, *329*, 515–523.

(17) Frisch, M. J. et al. *Gaussian 03*; Revision B.04; Gaussian, Inc.: Pittsburgh, PA, 2003.

(18) Labanowski, J. W.; Andzelm, J. *Density Functional Methods in Chemistry*; Springer: New York, 1991.

(19) Villamena, F. A.; Liu, Y.; Zweier, J. L. *J. Phys. Chem. A* **2008**, *112*, 12607–12615.

(20) Scott, A. P.; Radom, L. *J. Phys. Chem.* **1996**, *100*, 16502–16513.

(21) (a) Cossi, M.; Barone, V.; Cammi, R.; Tomasi, J. *J. Chem. Phys. Lett.* **1996**, *255*, 327. (b) Cossi, M.; Barone, V. *J. Chem. Phys.* **1998**, *109*, 6246. (c) Tomasi, J.; Persico, M. *Chem. Rev.* **1994**, *94*, 2027.

(22) Reed, A. E.; Weinhold, F. A.; Curtiss, L. A. *Chem. Rev.* **1998**, *98*, 899.

(23) Krenske, E. H.; Schiesser, C. H. *Org. Biomol. Chem.* **2008**, *6*, 854–859.

(24) Reed, A. E.; Curtiss, L. A.; Weinhold, F. A. *Chem. Rev.* **1988**, *88*, 899–926.

(25) Rockenbauer, A.; Clement, J.-L.; Culcasi, M.; Mercier, A.; Tordo, P.; Pietri, S. *J. Phys. Chem. A* **2007**, *111*, 4950–4957.

(26) Villamena, F. A.; Hadad, C. M.; Zweier, J. L. *J. Phys. Chem. A* **2005**, *109*, 1662–1674.

(27) Modro, A. M.; Modro, T. A. *Can. J. Chem.* **1999**, *77*, 890–894.

(28) Stolze, K.; Udilova, N.; Rosenau, T.; Hofinger, A.; Nohl, H. *Biol. Chem.* **2003**, *384*, 493.

(29) Frejaville, C.; Karoui, H.; Tuccio, B.; Le Moigne, F.; Culcasi, M.; Pietri, S.; Lauricella, R.; Tordo, P. *J. Chem. Soc., Chem. Commun.* **1994**, 1793–1794.